Supplement of Atmos. Chem. Phys., 26, 3107–3123, 2026
https://doi.org/10.5194/acp-26-3107-2026-supplement

Atmospheric Chemistry and Physics
Open Access
EGU

Supplement of

In-tandem multi-waveband particulate absorption and size observations yield substantial changes in radiative forcing over industrial Central China

Luoyao Guan et al.

Correspondence to: Jason Blake Cohen (jasonbc@alum.mit.edu)

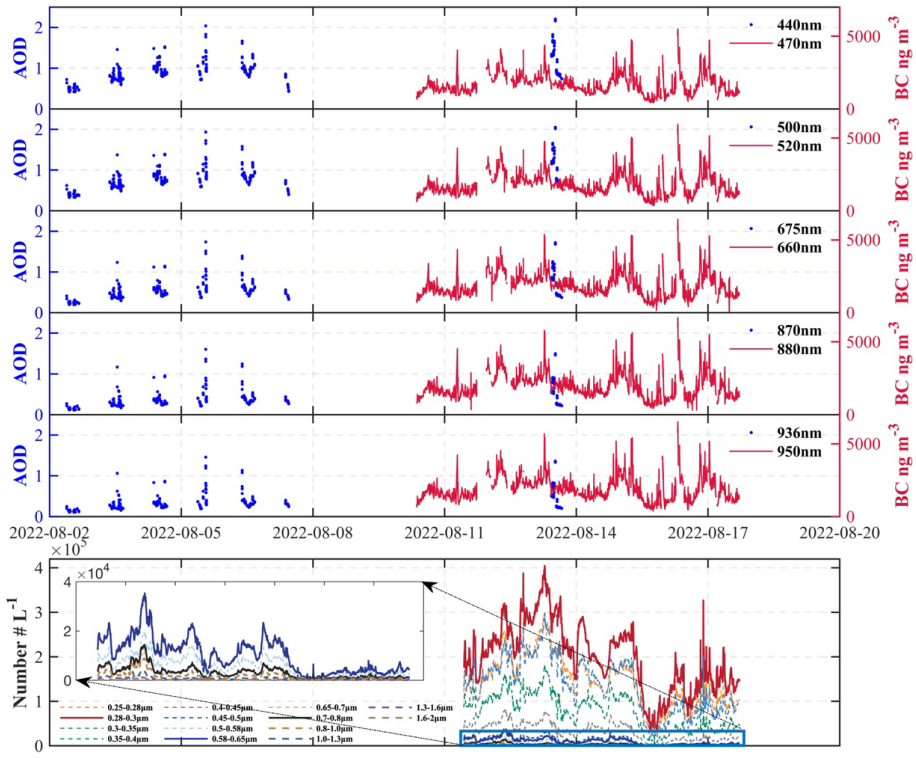

Figure S1: The measurements of field experiment campaign in August, 2022.

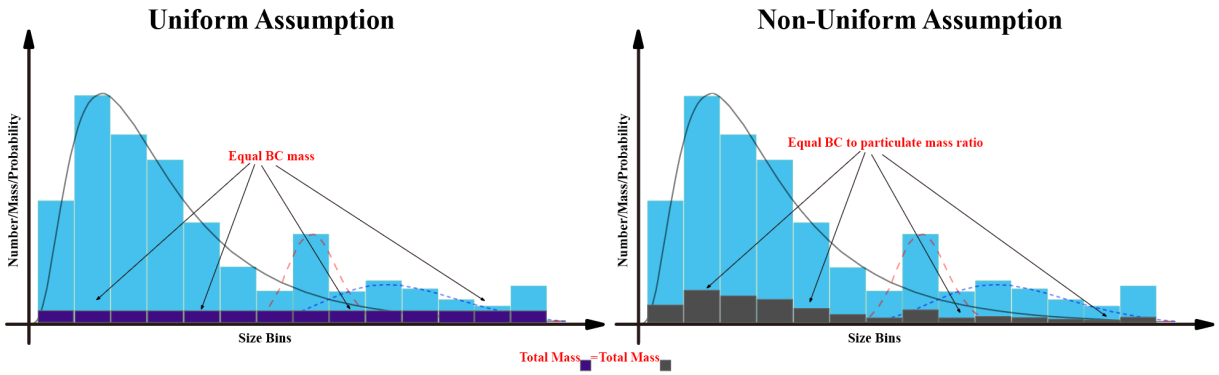

Figure S2. Schematic illustration of the uniform and non-uniform BC mixing-state assumptions used in this study, showing different allocations of BC mass across particle size bins under identical total BC mass.

Table S1: Summary of statistical metrics used in this study and their interpretive roles in constraining aerosol optical properties and TOA radiative forcing.

Statistical Index	Quantified Uncertainty / Information	Physical Interpretation	Manuscript Reference
RMSE	Forcing difference due to simplified size distributions (Log_1, Log_{123}) relative to ISSIZE reference	Indicates sensitivity of TOA forcing to aerosol size representation	Table 1
RMSE	Prediction error from statistical forcing estimates relative to Mie-SBDART results	Separates statistical modeling error from aerosol microphysical uncertainty	Table 2
R^2	Fraction of forcing variability explained by aerosol number, size, and spectral absorption	High R^2 suggests forcing variability is physically driven rather than noise-dominated	Table2; Figures 6
Two-tailed t-test	Statistical significance of wavelength-dependent forcing differences	Confirms that wavelength-dependent forcing differences are systematic	Section 3.3

Figure S3: Photograph taken by Luoyao Guan in the study areas in August, 2022. These are typical scenes associated with black carbon, coal dust, and absorbing aerosol emissions. (a) the environment of coal mining areas; (b) coal-fired power plants; (c) coal transportation (d) coal storage.

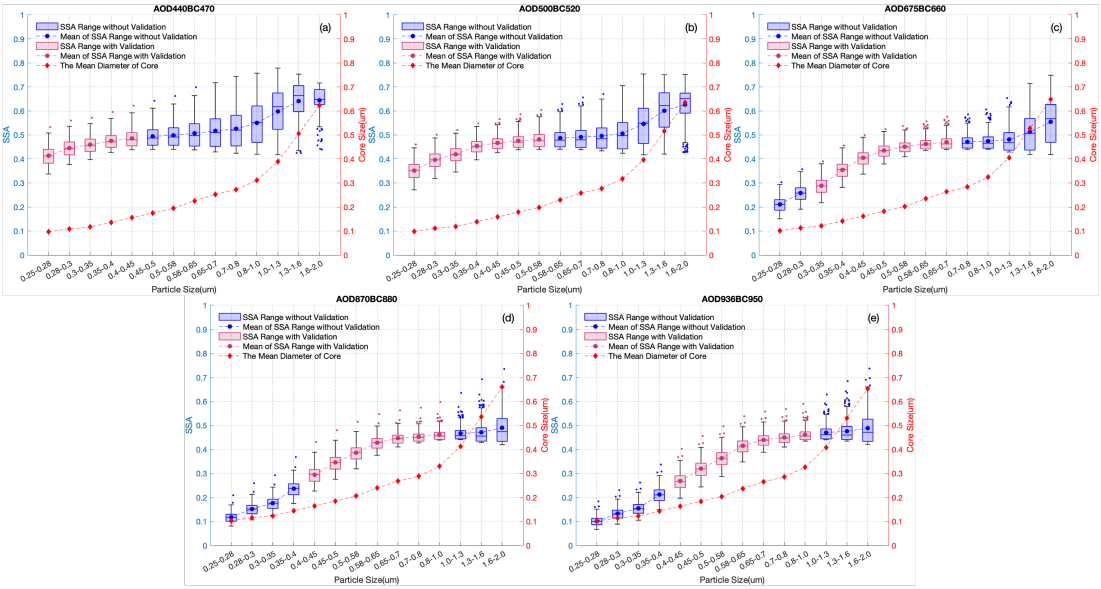

Figure S4: Multi-wavelength SSA simulation results under non-uniform assumption and ISSIZE distribution. Convex hull (pink) represents the particle size range where AAE theory is applicable, while concave hull (blue) indicates the non-applicable region, when computed using observations at (a) 470 nm; (b)520 nm; (c)660 nm; (d)880 nm; and (e)950 nm respectively.

20

Table S2. Comparison of aerosol optical representations in OPAC, AERONET, and this study, including size dependence, mixing assumptions, and typical SSA ranges.

Approach	Optical property treatment	Size dependence	Mixing assumption	Typical SSA range
OPAC	Prescribed optical properties based on idealized aerosol types	Fixed (Lognormal)	External or simplified internal mixing.	0.85-0.95
AERONET	Retrieved effective SSA from sun-sky radiance inversion	Implicit using two lognormal distributions (one in the coarse mode and one in the fine mode)	Implicit (core shell mixing is applied, using a fixed ratio between core and shell as a single effective mixing state)	0.85-0.92
This study	Observation-constrained, multi-wavelength inversion	Explicit, size-resolved: based on observations; a simplified three lognormal distribution; and a more simplified single lognormal distribution.	Core-shell mixing with flexible core to shell ratios.	0.28-0.85

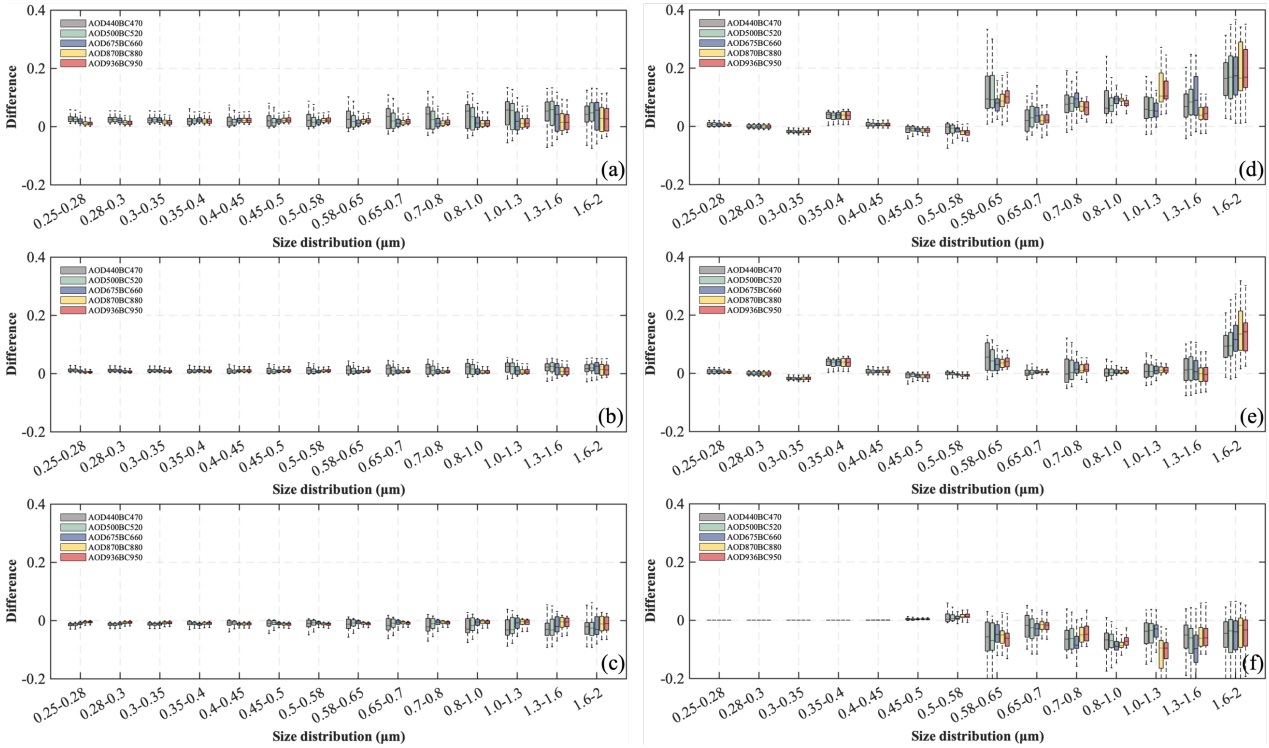

Figure S5: Differences of multiband SSA under different assumptions and size distributions. (a) ISSIZE and Log_1 under the non-uniform assumption; (b) ISSIZE and Log_{123} under the non-uniform assumption; (c) Log_1 and Log_{123} under the non-uniform assumption; (d) ISSIZE and Log_1 under the uniform assumption; (e) ISSIZE and Log_{123} under the uniform assumption;(f) Log_1 and Log_{123} under the uniform assumption.

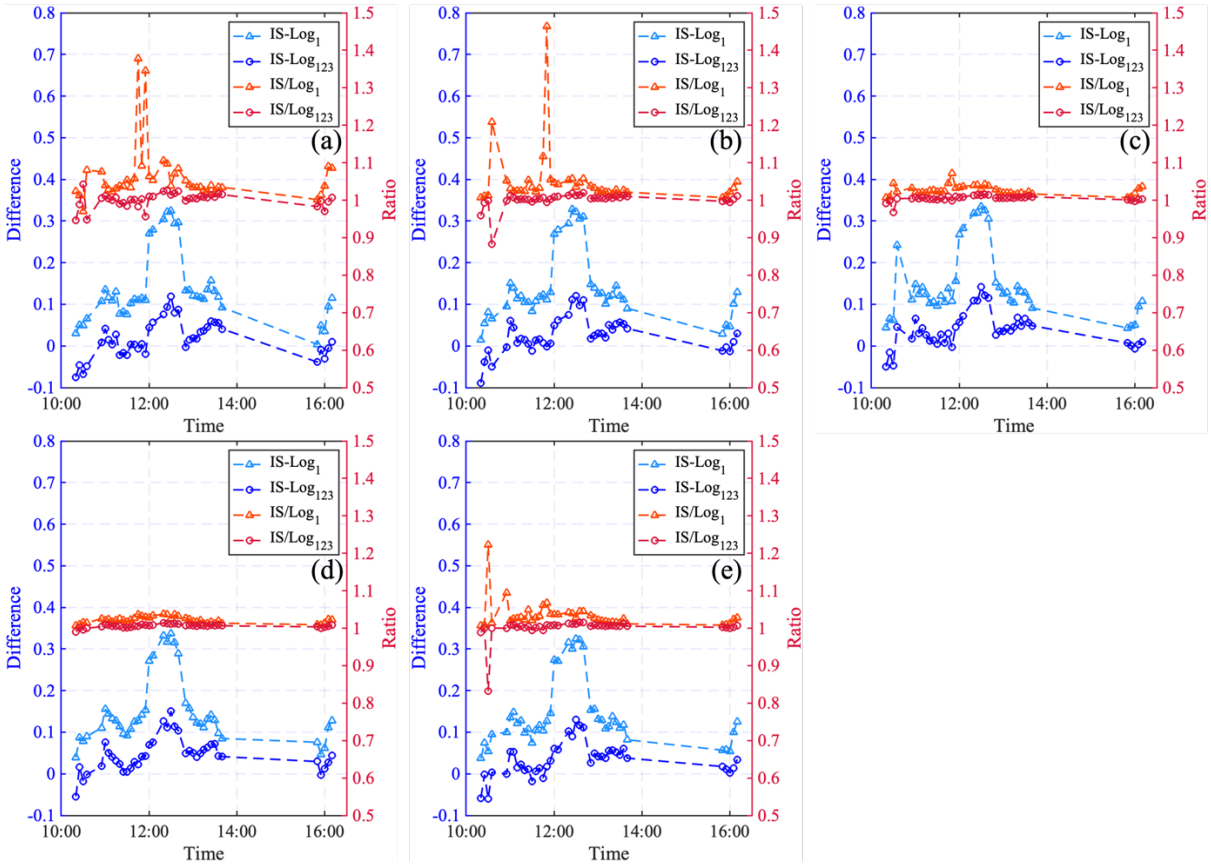

Figure S6: Differences of multiband radiative forcing and ratio with uniform assumption between different size distributions. (a) 470nm; (b)520nm; (c)660nm; (d)880nm; (e)950nm.

Table S3: The statistic of radiative forcing through all five bands with uniform assumption, the mean values of RF are given in bold, the standard deviations are given in parentheses, the last two rows are RMSE between different size distribution.

	470 nm	520 nm	660 nm	880 nm	950 nm
ISSIZE	**3.1**(*1.9*)	**4.5**(*2.0*)	**6.1**(*2.3*)	**6.9**(*2.2*)	**5.7**(*2.4*)
Log_1	**3.0**(*1.9*)	**4.4**(*2.0*)	**5.9**(*2.3*)	**6.8**(*2.1*)	**5.5**(*2.3*)
Log_{123}	**3.1**(*1.9*)	**4.5**(*2.0*)	**6.0**(*2.3*)	**6.9**(*2.1*)	**5.6**(*2.3*)
RMSE(ISSIZE-Log_1)	0.16	0.16	0.18	0.17	0.16
RMSE(ISSIZE-Log_{123})	0.05	0.05	0.06	0.06	0.05

Table S4: The statistic of two first-order linear/non-linear models with uniform assumption through all five wavelengths, the coefficient of determination is given in bold, the RMSE, and weighted RMSE are given in parentheses (W m^{-2}).

	470 nm	520 nm	660 nm	880 nm	950 nm
ISSIZE (SSA)	**0.79**(*4.44, 0.09*)	**0.76**(*4.39, 0.09*)	**0.73**(*4.28, 0.09)*	**0.71**(*4.20, 0.10*)	**0.74**(*4.34, 0.09*)
Log_1 (SSA)	**0.85**(*4.31, 0.10*)	**0.85**(*4.1, 0.11*)	**0.85**(*3.97, 0.12*)	**0.83**(*4.07, 0.12*)	**0.86**(*3.92, 0.11*)
Log_{123} (SSA)	**0.82**(*4.40, 0.09*)	**0.81**(*4.35, 0.09*)	**0.79**(*4.30, 0.11*)	**0.77**(*4.32, 0.11*)	**0.80**(*4.28, 0.10*)
ISSIZE (SSA, AOD, size)	**0.93**(*2.73, 0.06*)	**0.93**(*2.61, 0.07*)	**0.93**(*2.5, 0.07*)	**0.93**(*2.39, 0.07*)	**0.93**(*2.56, 0.06*)
Log_1 (SSA, AOD, size)	**0.93**(*2.98, 0.12*)	**0.93**(*2.73, 0.07*)	**0.94**(*2.57, 0.07*)	**0.93**(*2.57, 0.08*)	**0.94**(*2.57, 0.07*)
Log_{123} (SSA, AOD, size)	**0.93**(*2.87, 0.14*)	**0.93**(*2.72, 0.15*)	**0.92**(*2.55, 0.16*)	**0.92**(*2.49, 0.15*)	**0.93**(*2.51, 0.07*)

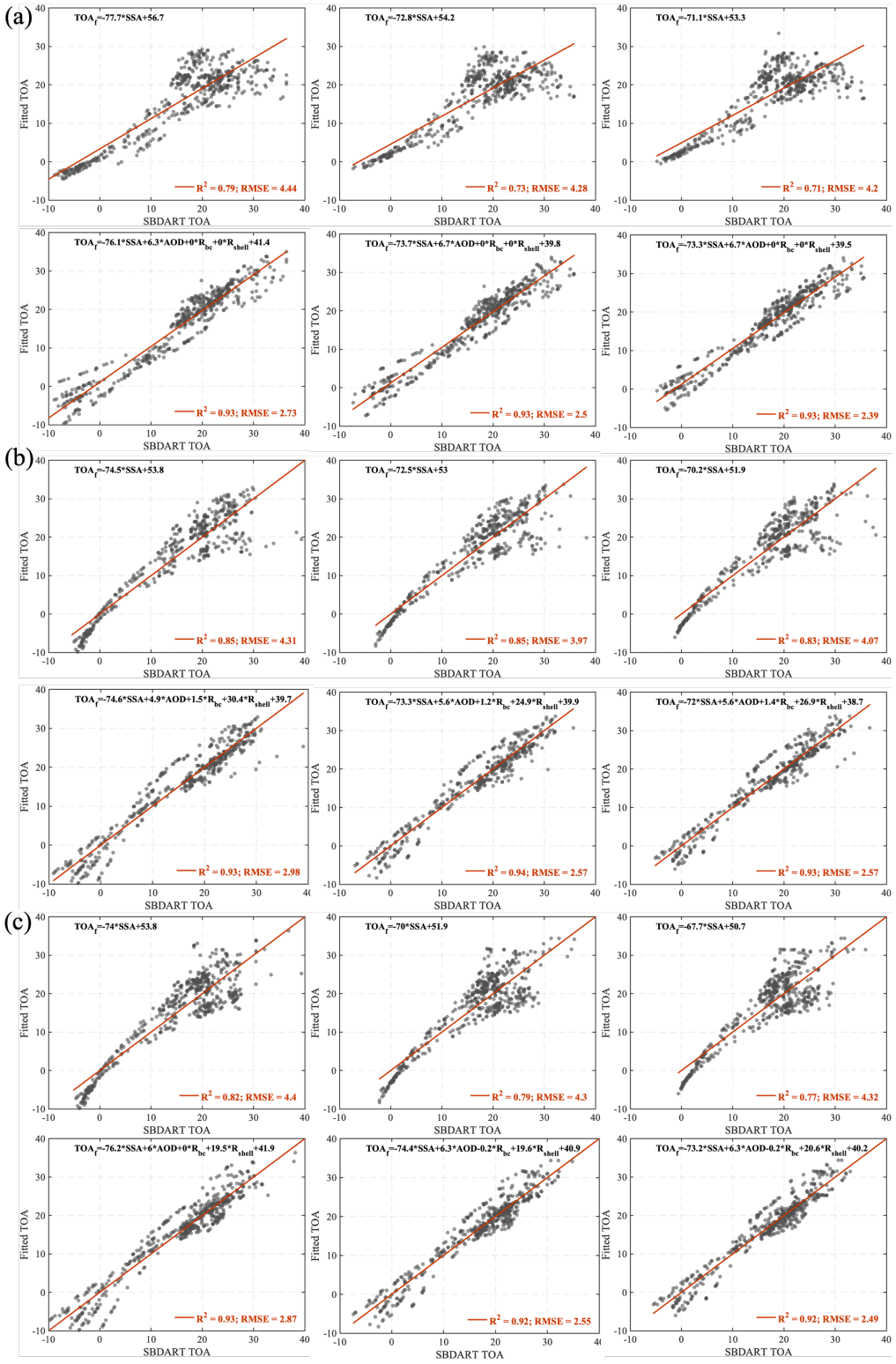

Figure S7: Deriving adjusted TOA using two different linear models with uniform assumption, the first row in each subfigure is linear model only including SSA, the second row is linear model including the effects of BC core, sulfate shell and AOD as additional variables, the first to the third column for each subfigure is 470nm, 660nm and 880nm. (a) ISSIZE measurements; (b)Log_1 distribution; (c)Log_{123} distribution.